Catalysis Today 149 (2010) 148–156

Contents lists available at ScienceDirect

Catalysis Today

journal homepage: www.elsevier.com/locate/cattod

Influence of catalyst pretreatment on catalytic properties and performances of Ru–Re/SiO_2 in glycerol hydrogenolysis to propanediols

Lan Ma [a,b], Dehua He [a,*]

[a] Innovative Catalysis Program, Key Lab of Organic Optoelectronics & Molecular Engineering of Ministry of Education, Department of Chemistry, Tsinghua University, Beijing 100084, China
[b] Institute of Chemical Defence, Beijing 102205, China

ARTICLE INFO

Article history:
Available online 15 May 2009

Keywords:
Glycerol hydrogenolysis
Ru–Re/SiO_2
Re promoting effect
Pretreatment

ABSTRACT

Bimetallic Ru–Re/SiO_2 and monometallic Ru/SiO_2 catalysts were prepared by impregnation method and their catalytic performances were evaluated in the hydrogenolysis of glycerol to propanediols (1,2-propanediol and 1,3-propanediol) with a batch type reactor (autoclave) under the reaction conditions of 160 °C, 8.0 MPa and 8 h. Ru–Re/SiO_2 showed much higher activity in the hydrogenolysis of glycerol than Ru/SiO_2, and the pretreatment conditions of the catalyst precursors had great influence on the catalytic performance of both Ru–Re/SiO_2 and Ru/SiO_2 catalysts. The physicochemical properties of Ru–Re/SiO_2 and Ru/SiO_2, such as specific surface areas, crystal phases, morphologies/microstructures, surface element states, reduction behaviors and dispersion of Ru metal, were characterized by N_2 adsorption/desorption, XRD, Raman, TEM–EDX, XPS, H_2-TPR and CO chemisorption. The results of XRD, TEM–EDX and CO chemisorption characterizations showed that Re component had an effect on promoting the dispersion of Ru species on the surface of SiO_2, and the measurements of H_2-TPR revealed that the co-existence of Re and Ru components on SiO_2 changed the respective reduction behavior of Re or Ru alone. High pre-reduction temperatures would decrease the activities of Ru–Re/SiO_2 and Ru/SiO_2 catalysts, compared with the corresponding calcined catalysts (without pre-reduction), which actually went through an in-situ reduction during the reaction. XPS analysis indicated that Ru species was in Ru^0 metal state, while Re species was mostly in Re oxide state in the spent Ru–Re/SiO_2 sample. Re component was probably in rhenium oxide state rather than Re^0 metal state to take part in the reaction via interaction with Ru^0 metal.

1. Introduction

Bio-diesel has been considered as a kind of environment friendly fuel because it is ultra clean and makes a certain contribution to gaining energy sustainability. With the increase of bio-diesel production, the development of down-stream products of glycerol, the by-product of bio-diesel production, has recently attracted much attention because it is a low-cost renewable feedstock [1,2]. Glycerol can be converted to other high added-value chemicals by catalytic processes, such as to propanediols by the hydrogenolysis of glycerol [3,4], to glyceric acid by the oxidation of glycerol [5], to acrolein by the dehydration of glycerol [6]. Propanediols, both 1,2-propanediol and 1,3-propanediol, are important chemicals in industry. 1,2-propanediol is a non-toxic chemical material and it can be used as a humectant, antifreeze, brake fluid and humectant, or as a component of polyesters and alkyd resins [7]. 1,3-propanediol is usually used for the manufacture of plasticizer, abluent, corrosion remover, paint and copolymers, especially for the production of polyester (polytrimethylene terephthalate) with terephthalic acid [7]. However, both 1,2-propanediol and 1,3-propanediol are produced via petroleum routes in industrially at present. Therefore, the production of them from renewable resources is highly desired [7].

Several researches have recently focused on the conversion of glycerol to propanediols by catalytic hydrogenolysis method, and some heterogeneous catalysts, such as Cu-based catalysts [3,8], Raney-nickel catalysts [8,9], Ru-based catalysts [4,10], and other noble metal (Rh, Pt, Au, etc.) catalysts [11–13], have been employed. Ru has been considered to be an effective catalytic component in glycerol hydrogenolysis. Miyazawa et al. reported that the combination of 5%Ru/C and Amberlyst-15 resin was effective for the glycerol hydrogenolysis to 1,2-propanediol, compared with the combinations of the other noble metal catalysts (Rh/C, Pt/C and Pd/C) and acid promoters (Amberlyst-15, H_2SO_4 and HCl) [4]. Some base additives (NaOH and CaO) could increase the activity of Ru/C and Pt/C catalysts [13]. However, it can be seen

* Corresponding author. Tel.: +86 10 62773346; fax: +86 10 62773346.
E-mail address: hedeh@mail.tsinghua.edu.cn (D. He).

0920-5861/$ – see front matter © 2009 Elsevier B.V. All rights reserved.
doi:10.1016/j.cattod.2009.03.015

that the activity and selectivity for the glycerol hydrogenolysis to propanediols with Ru catalysts alone are still not satisfying. The modification of Ru catalysts for improving their performance in the hydrogenolysis of glycerol is necessary. It has been reported that bimetallic catalysts can be superior to monometallic catalysts in the catalytic activity and selectivity for many reactions [14]. Maris et al. applied bimetallic PtRu/C and AuRu/C catalysts to the aqueous-phase hydrogenolysis of glycerol at 473 K and 40 bar H_2 and found that the PtRu catalyst appeared to be stable under the aqueous-phase reaction conditions, but it seems that the activity and selectivity of AuRu/C or PtRu/C in the hydrogenolysis of glycerol was similar to the monometallic Ru/C [12,13]. Generally, the synergistic effect of bimetals and the interaction between metal and support could be influenced by the preparation methods and pretreatments of catalysts, which in turn affect the catalytic performance of the catalysts [15–22]. For Pt–Re/Al_2O_3 reforming catalysts, it has been reported that bimetallic particles of platinum and rhenium could be formed when the catalyst was dried in air at temperatures $\leq$500 °C before reduction at 480 °C [15]. On the other hand, the degree of surface hydroxylation of Al_2O_3 in Pt–Re/Al_2O_3 reforming catalysts essentially affected aggregation or segregation of Pt and Re during reduction step [16]. Thus, pretreatments at severe conditions could lead to dehydroxylation of the alumina surface and result in Pt–Re segregation, while pretreatments at moderate conditions preserved surface hydroxyl groups, which favored the transport of ReOx species to Pt during the reduction step, and resulted in the aggregation of metals [16]. Epron et al. found that the interactions between platinum and copper on a Pt–Cu bimetallic catalyst were noticeably affected by reducing and oxidizing pretreatments, and consequently the catalytic activity for nitrate reduction in water was changed [17].

In our previous work, we found a remarkable promoting effect of Re component on the activity of Ru catalysts in the hydrogenolysis of glycerol to propanediols [23], and investigated the behaviors of Ru–Re bimetallic catalysts in the hydrogenolysis of glycerol and confirmed the significant synergistic effect of Ru and Re on increasing the activity of the catalysts [24]. Recently, we also found that the preparation parameters could obviously affect the catalytic performance of Ru–Re bimetallic catalysts and corresponding Ru monometallic catalysts. In this paper, we focus on the influence of pretreatment of Ru–Re/SiO_2 and Ru/SiO_2 precursors on catalytic performance in glycerol hydrogenolysis to propanediols.

2. Experimental

2.1. Catalyst preparation

SiO_2 was obtained from Tianjin Chemical Institute and used as a support, which was calcined at 400 °C for 4 h before used. $Re_2(CO)_{10}$ was purchased from Stream Company and used as received. $RuCl_3{\cdot}4H_2O$ and $HReO_4$, which were purchased from Institute of ShenYang Youse Jinshu and Alfa Aesar Company, respectively, were used for preparing Ru/SiO_2, Re/SiO_2 and Ru–Re/SiO_2 bimetallic catalysts.

Supported monometallic catalysts (Ru/SiO_2 and Re/SiO_2) and bimetallic Ru–Re/SiO_2 catalyst were prepared by impregnation method. The powder of SiO_2 was impregnated with $RuCl_3{\cdot}4H_2O$ or $HReO_4$ aqueous solution or the mixture aqueous solution of $RuCl_3{\cdot}4H_2O$ and $HReO_4$. After impregnation and solvent removal by evaporation, the precursors were dried at 110 °C for 12 h, and calcined at 350 °C in air for 5 h. The calcined samples were denoted as Ru/SiO_2-c350, Re/SiO_2-c350 and Ru–Re/SiO_2-c350. Some calcined samples were further reduced in H_2–N_2 flow (H_2/N_2 = 3/5, 80 ml/min) at 450 °C (or 300, 200 °C) for 4 h, and finally passivated in a flowing of CO_2–N_2 gas (CO_2/N_2 = 2/5, 70 ml/min) for 12 h and stored in the desiccator. The samples reduced by H_2–N_2 flow were denoted as Ru/SiO_2-r*T* and Ru–Re/SiO_2-r*T*, and here "*T*" refers to the pre-reduction temperatures (450, 300, 200 °C). The actual loading of Ru and Re on the catalysts was analyzed by Inductive Coupling Plasma-Atomic Emission Spectroscopy (ICP-AES), that is, 3.55% Ru/SiO_2, 3.23% Ru-3.57% Re/SiO_2 and 4.01% Re/SiO_2.

2.2. Characterization of catalysts

The specific surface areas, cumulative pore volume and average pore diameter of the catalysts and supports were measured by N_2 adsorption/desorption with the BET and BJH methods on a Micromeritics ASAP 2010C analyzer. Before measurement, the samples were degassed at 200 °C for 2 h. The phase structures of the catalysts were determined by X-ray Diffraction (XRD) with a Bruker D8 Advance X-Ray Powder Diffractometer with Cu Kα (λ = 0.15406 nm). The crystal sizes of metal or metal oxides were determined by means of the X-ray line broadening method according to the well-known Scherrer formula. Raman spectra were recorded at room temperature on a Microscopic Confocal Raman spectrometer (Renishaw, RM 2000) equipped with Ar^+ laser. The 633 nm line from an argon ion laser was used as the excitation source. The laser was operated at a power of 15 mW. The morphologies and microstructure of the catalysts were characterized by high-resolution transmission electron microscopy (HR-TEM, JEM-2010 of JEOL) equipped with an energy dispersive X-ray detector (EDX). The accelerating voltage was 120 kV. The samples were ultrasonically dispersed in ethanol and deposited on a holey carbon copper grid before measurement. The X-ray photoelectron spectroscopy (XPS) measurements were performed on a PHI Quantera Scanning X-ray Microprobe of ULVAC-PHI Inc. The spectra were referenced with respect to C 1s line at 284.8 eV.

Temperature-programmed reduction (TPR) measurements were carried out on a dynamic-flow gas sorption instrument (Quantachrome, CHEMBET 3000 TPR/TPD). The catalyst samples (about 100 mg) were treated in Ar at 350 °C for 0.5 h before TPR was performed. All TPR measurements were carried out in a flow of 4.97% H_2/Ar (20 ml/min) at a heating rate of 15 °C/min. A cold trap (liquid nitrogen + iso propanol) was placed before the TCD to remove water produced during TPR measurements. The hydrogen consumption was calibrated using TPR of copper oxide (CuO) at the same conditions.

The dispersion of Ru metal on supports was measured by CO chemisorption method. CO chemisorption was operated on dynamic-flow gas sorption instrument (Quantachrome, CHEMBET 3000 TPR/TPD). Before CO chemisorption was performed, catalyst samples (about 200 mg) were treated in a quartz reactor in a flow of H_2 (20 ml/min) at 400 °C for 2 h and then purged in He flow. The temperature of samples was decreased to 40 °C in He flow. The CO chemisorption was performed by pulse injection of pure CO gas at 40 °C. The stoichiometry of CO to Ru was 1 for CO chemisorption [25].

2.3. Hydrogenolysis reaction of glycerol

The hydrogenolysis of glycerol (ultra pure, Alfa Aesar Company) was carried out in a stainless steel autoclave of 100 ml with a magnetic stirrer. Detailed procedure was described in our previous paper [23]. The standard reaction conditions were 160 °C, 8 MPa hydrogen pressure and 8 h reaction time, using 10 ml 40 wt% glycerol aqueous solution and 0.15 g supported catalyst in every run. After the reaction, the liquid and the solid catalyst in the mixture were separated by centrifugation and filtration.

The products in liquid phase were analyzed qualitatively by GC–MS (GCMS-QP2010, SHIMADZU Corporation) and analyzed

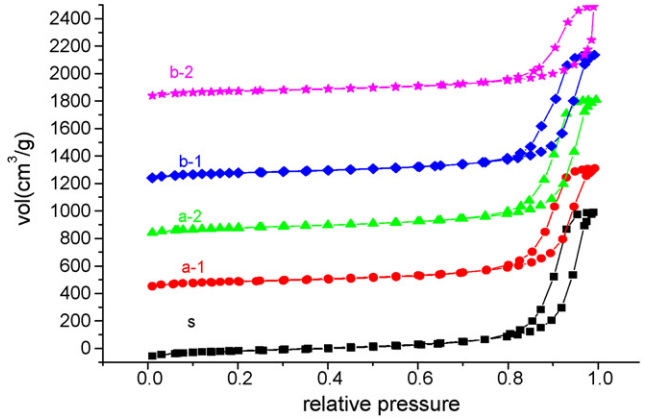

Fig. 1. Adsorption/desorption isotherms of samples. (s) SiO_2; (a-1) Ru/SiO_2-c350; (a-2) Ru/SiO_2-r450; (b-1) $Ru–Re/SiO_2$-c350; (b-2) $Ru–Re/SiO_2$-r450.

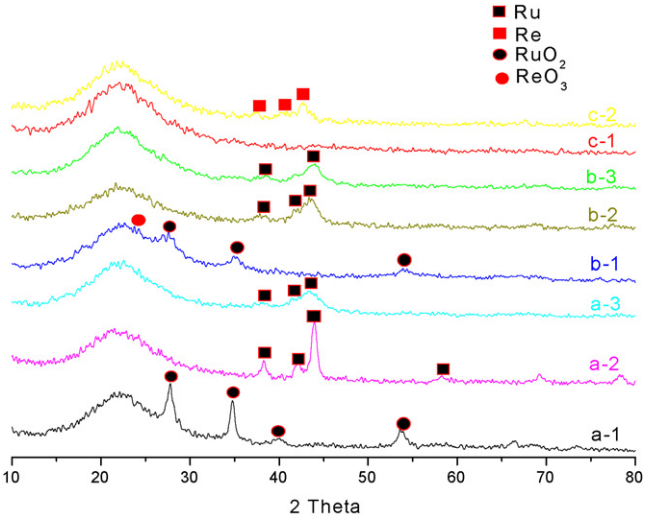

Fig. 2. XRD patterns of catalysts (a-1) Ru/SiO_2-c350; (a-2) Ru/SiO_2-r450; (a-3) spent Ru/SiO_2-c350; (b-1) $Ru–Re/SiO_2$-c350; (b-2) $Ru–Re/SiO_2$-r450; (b-3) spent $Ru–Re/SiO_2$-c350; (c-1) Re/SiO_2-c350; (c-2) Re/SiO_2-r450 (Data of No. a-1, a-3, b-1, b-2 and c-1 are from reference [24]).

quantitatively with a gas chromatography (Lunan-SP 6890, PEG2M, 30 m × 0.25 mm; FID detector). The products in gas phase was not quantitatively analyzed, but qualitatively checked with a GC (TDX-01, TCD).

The conversion in present study is denoted as "conversion of glycerol to liquid products" (shorted as conversion of glycerol, hereafter). The selectivity is denoted as "selectivity in liquid products" (shorted as selectivity, hereafter). The conversion of glycerol and the selectivity of each liquid product in all runs in present study were calculated based on the following equations.

$$\text{Conversion of glycerol}\,(\%) \frac{\text{Sum of} C_{\text{mol}} \text{ of all liquid products}}{\text{Added glycerol before reaction}\,(C_{\text{mol}})} \times 100.$$

$$\text{Selectivity}\,(\%) = \frac{C_{\text{mol}} \text{ of each liquid product}}{\text{Sum of} C_{\text{mol}} \text{ of all liquid products}} \times 100.$$

3. Results and discussion

3.1. Characterization of catalysts

3.1.1. N_2 adsorption/desorption isotherms and texture structure measurement

N_2 adsorption/desorption isotherms of support SiO_2, monometallic Ru/SiO_2 and bimetallic $Ru–Re/SiO_2$ catalysts are presented in Fig. 1, and the relative texture parameters (specific surface areas (S_{BET}), cumulative pore volume and average pore diameter) of these samples are also listed in Table 1. All the samples shown in Fig. 1 exhibited type IV isotherms, and the pore structure of SiO_2 was kept no obvious change after supporting metal elements on the support. SiO_2 showed high specific surface area (S_{BET} = 301 m^2/g) and had large cumulative pore volume and average pore diameter. The S_{BET} decreased when metal components were supported on the support and calcined at 350 °C for 4 h, while the change of cumulative pore volume and average pore diameter were not obvious. The S_{BET} of reduced Ru/SiO_2 was almost same as that of calcined Ru/SiO_2, while S_{BET} of reduced $Ru–Re/SiO_2$ decreased somewhat compared with calcined $Ru–Re/SiO_2$.

Table 1
Specific surface areas, pore volume and average pore diameter of samples.

Catalyst	Specific surface area (m^2/g)[a]	Cumulative pore volume (cm^3/g)[a]	Average pore diameter (nm)[a]	Crystal size (nm)
SiO_2[c]	301	1.69	19	15
Ru/SiO_2-c350	286	1.40	17	16 (RuO_2)[b]
Ru/SiO_2-r450[c]	284	1.56	18	18 (Ru^0)[b]
$Ru–Re/SiO_2$-c350	285	1.45	18	–
$Ru–Re/SiO_2$-r450[c]	268	1.20	19	–

[a] By N_2 adsorption/desorption method.
[b] By X-ray line broadening method using Scherrer formula.
[c] Data from reference [24].

3.1.2. X-ray diffraction and Raman spectra measurement

The results of XRD characterization of the fresh and spent catalysts are presented in Fig. 2. The calcined Ru monometallic catalyst (Ru/SiO_2-c350) showed typical RuO_2 diffraction peaks [JCPDS File 40-1290] in the XRD profile of Ru/SiO_2-c350 (Fig. 2, a-1), indicating that there were well-crystallized RuO_2 [26] particles on SiO_2 support. And after being reduced, typical Ru^0 diffraction peaks [JCPDS File 06-0663] could be observed from the XRD profile of Ru/SiO_2-r450 (Fig. 2, a-2), indicating that Ru metal crystal phase was formed. The crystal sizes of RuO_2 and Ru^0 on the catalysts were determined by means of the X-ray line broadening method using Scherrer formula and the results are shown in Table 1. The crystal size of RuO_2 on the Ru/SiO_2-c350 catalyst was 16 nm, while the particle sizes of Ru^0 on the Ru/SiO_2-r450 was 18 nm, indicating that the average crystal size of Ru species increased somewhat after being reduced in flowing H_2 at 450 °C. After Ru/SiO_2-c350 catalyst went through the hydrogenolysis of glycerol at 160 °C and 8.0 MPa H_2 for 8 h, weak and broad diffraction peaks, which were assigned to Ru^0 [JCPDS File 06-0663] phase, were observed on the XRD profile of the spent Ru/SiO_2-c350 sample (Fig. 2, a-3), indicating that the well-crystallized RuO_2 on the surface of Ru/SiO_2-c350 sample went through an in-situ reduction during the hydrogenolysis reaction, and was reduced to Ru metal state.

On the other hand, for the calcined sample of Re/SiO_2, no diffraction peak was observed in the XRD profile of Re/SiO_2-c350 (Fig. 2, c-1), and this implies that Re species might be well dispersed on SiO_2 support. After being reduced in flowing H_2 at 450 °C, the weak diffraction peaks of Re^0 metal phase [JCPDS File 05-0702] could be seen from the XRD profile of Re/SiO_2-r450 (Fig. 2, c-2), implying that the well-dispersed rhenium oxide was reduced and crystallized in the reduction process.

When Ru and Re components were simultaneously supported on SiO_2, the diffraction peaks in the XRD profile of $Ru–Re/SiO_2$-c350 (Fig. 2, b-1), which were assigned to RuO_2 phase, were weaker

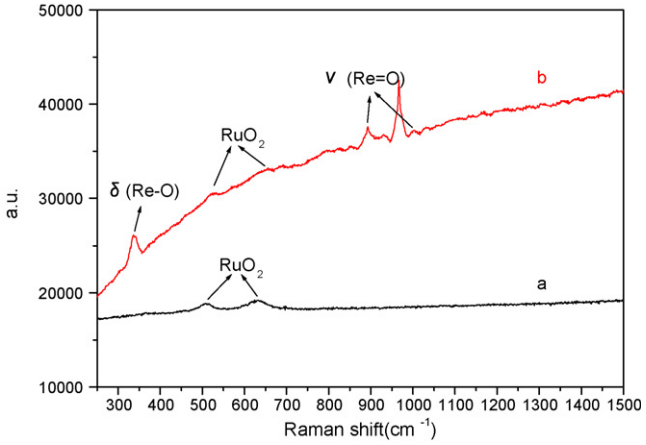

Fig. 3. Raman spectra of catalysts (a) Ru/SiO_2-c350, (b) $Ru–Re/SiO_2$-c350.

and broader compared with the case of Ru/SiO_2-c350 (Fig. 2, a-1). Furthermore, a very weak diffraction peaks at $2\theta \approx 24.1$, which could be assigned to ReO_3 phase [JCPDS File 84-0952] was also observed in the XRD profile of $Ru–Re/SiO_2$-c350 (Fig. 2, b-1). These results suggest that Ru and Re oxide particles might be well dispersed on the support when Ru and Re components were simultaneously supported on SiO_2, and Re component had an effect on promoting the dispersion of Ru component on the surface of SiO_2. Furthermore, the existence of rhenium oxide on the surface of $Ru–Re/SiO_2$-c350 was also confirmed by the characterization of Raman spectrometer (Fig. 3). The Raman spectrum of $Ru–Re/SiO_2$-c350 featured several bands, in which the peaks at 338, 895 and 1001 cm^{-1} (Fig. 3, b) were due to the Raman scattering of Re–O and Re=O [27]. However, the ascription of a strong peak at 965 cm^{-1} was still not clear, and perhaps it was originated from the interaction of Ru–Re oxide species. The Raman spectrum of Ru/SiO_2-c350 showed two peaks at 508 and 629 cm^{-1}, which could be assigned to the Raman scattering of RuO_2 species [28,29].

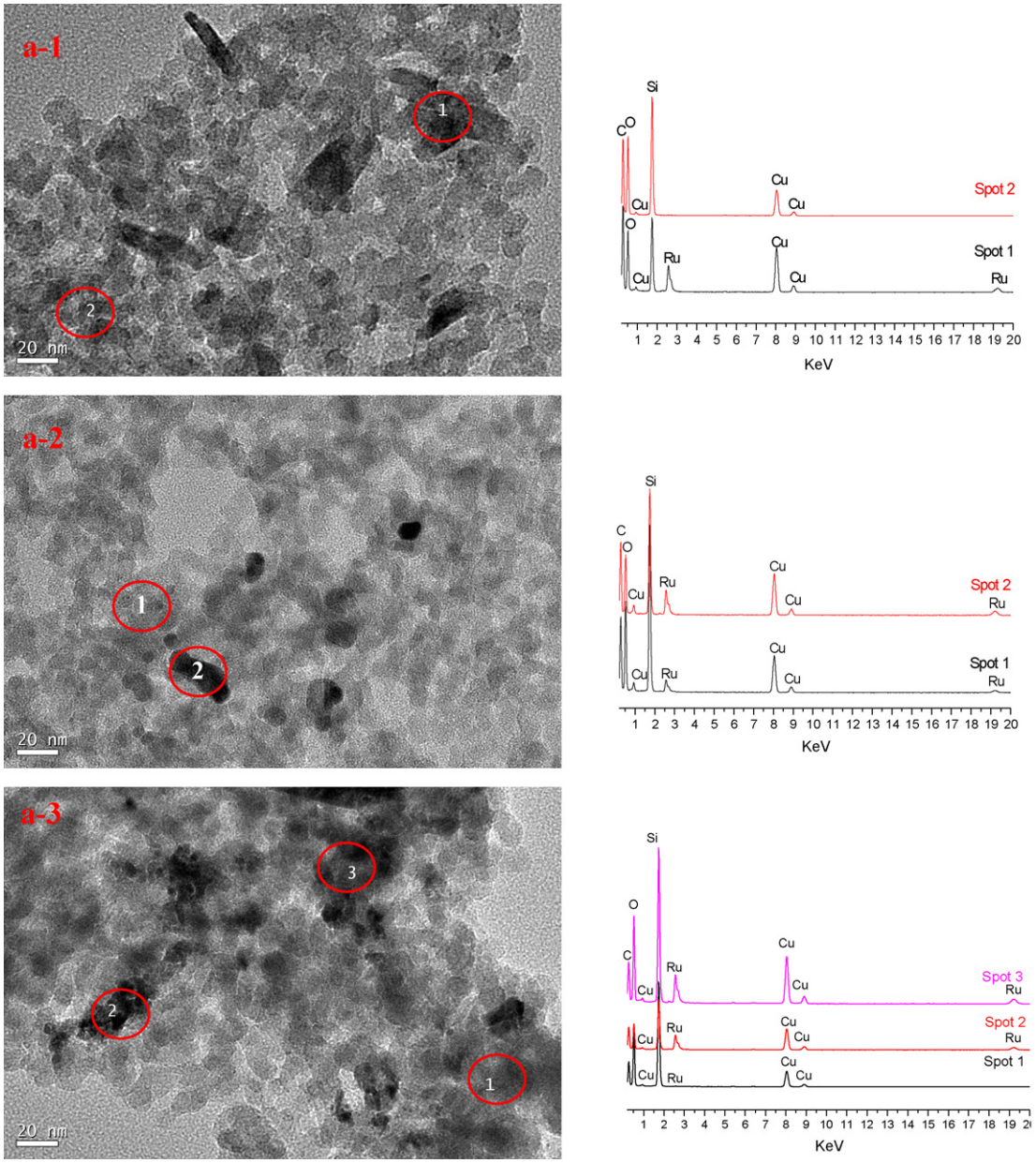

Fig. 4. HR-TEM images and EDX spectra of (a-1) Ru/SiO_2-c350; (a-2) Ru/SiO_2-r450; (a-3) spend Ru/SiO_2-c350; (b-1) $Ru–Re/SiO_2$-c350; (b-2) $Ru–Re/SiO_2$-r450 and (b-3) spend $Ru–Re/SiO_2$-c350.

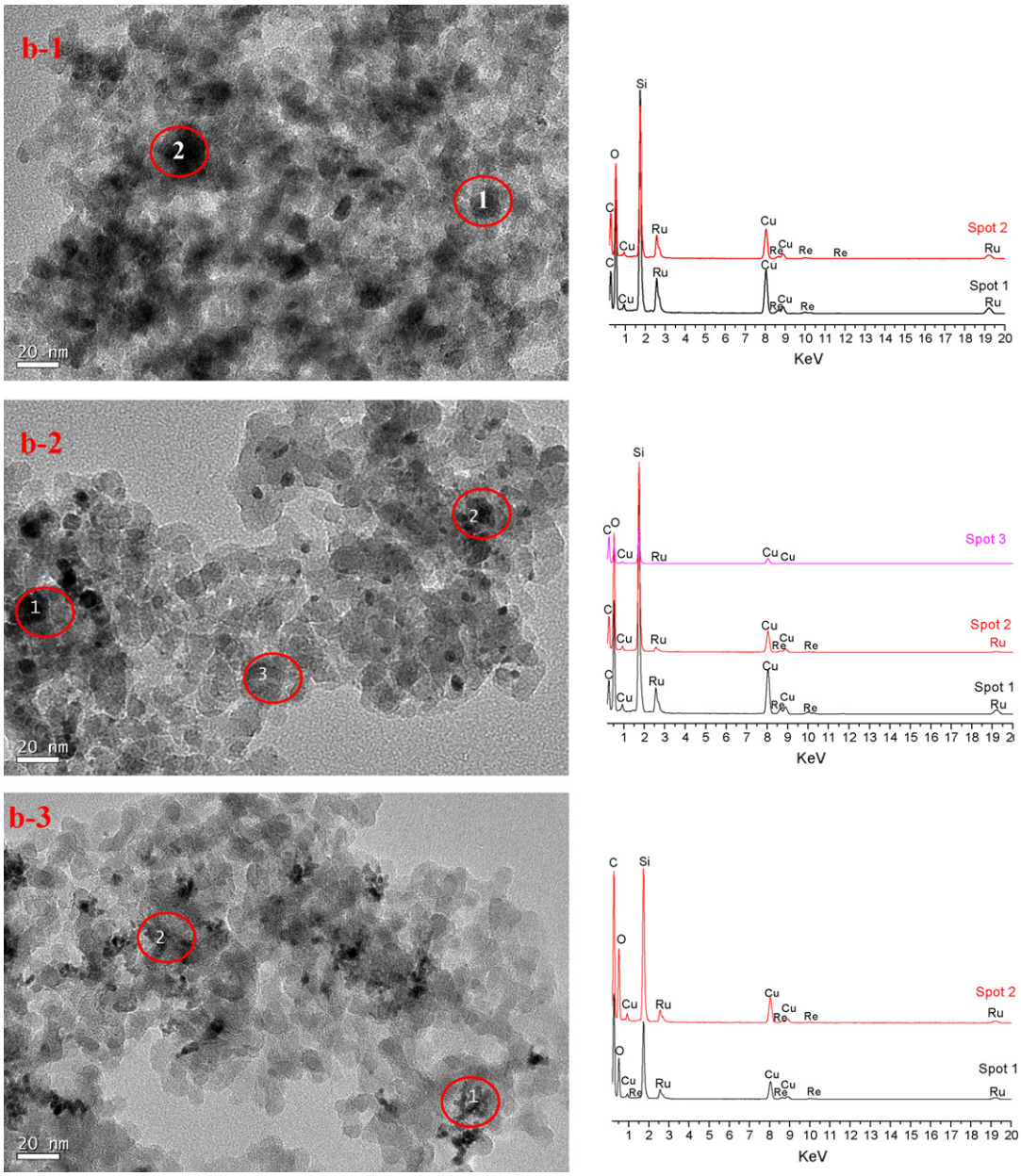

Fig. 4. (*Continued*).

When the sample of Ru–Re/SiO_2-c350 was reduced in flowing H_2 at 450 °C, the diffraction peaks of Ru^0 phase were observed in the XRD profile of Ru–Re/SiO_2-r450 (Fig. 2, b-2), and the peak intensity of Ru^0 metal phase on Ru–Re/SiO_2-r450 was stronger than that of RuO_2 phase on Ru–Re/SiO_2-c350 (Fig. 2, b-1), indicating that there existed an aggregation of metal particles on Ru–Re/SiO_2 during the reduction process. On the other hand, from the XRD result of Ru–Re/SiO_2-r450, it is difficult to estimate whether there existed a Re^0 metal crystal phase on the surface of Ru–Re/SiO_2-r450 or not, because the typical diffraction peak ($2\theta \approx 42.9$) of Re^0 metal was very closed to the typical diffraction peak ($2\theta \approx 44.1$) of Ru^0 metal and the Re^0 peak might be covered by the Ru^0 peak.

After the reaction, only weak and broad diffraction peaks of Ru^0 phase were observed in the XRD profile of spent Ru–Re/SiO_2-c350 (Fig. 2, b-3), confirming the occurrence of in-situ reduction of Ru–Re/SiO_2-c350 during the reaction. However, there was no diffraction peak assigned to the phases of Re species being detected on the spent Ru–Re/SiO_2-c350 catalyst, suggesting that Re species could be well dispersed on the surface of the catalyst even after the reaction. Furthermore, the diffraction peaks of Ru^0 phase on the spent Ru–Re/SiO_2-c350 were weaker and broader than that of Ru^0 phase on Ru–Re/SiO_2-r450, suggesting the dispersion of Ru^0 particles on the spent Ru–Re/SiO_2-c350 might be better.

Owing to the too weak and broad diffraction peaks of the samples of spent Ru/SiO_2-c350, Re/SiO_2-r450, Ru–Re/SiO_2-c350, Ru–Re/SiO_2-r450 and spent Ru–Re/SiO_2-c350, the average crystal sizes of Ru^0, Re^0, RuO_2 or ReO_3 phases could not be determined by the calculation using Scherrer equation.

3.1.3. HR-TEM and EDX analysis

The morphologies and microstructure of Ru/SiO_2 and Ru–Re/SiO_2 were characterized by HR-TEM. The images of TEM and the corresponding results of EDX analysis are shown in Fig. 4. For Ru/SiO_2-c350, some stick-shaped particles could be observed in its TEM image such as the area 1 in Fig. 4, a-1, which was confirmed to contain Ru species by EDX analysis. These results imply that RuO_2 was crystallized and not well dispersed on the surface of support

SiO_2. This is coincided with the results of XRD (Fig. 2, a-1) that the crystallized RuO_2 existed on the Ru/SiO_2-c350 catalyst.

On the other hand, when Ru/SiO_2-c350 was reduced in flowing H_2 at 450 °C, large Ru metal particles could be seen from the TEM image of Ru/SiO_2-r450 and the existence of Ru component on Ru/SiO_2-r450 was also confirmed by the EDX analysis (Fig. 4, a-2) in both black particle region and the bright contrast region in the TEM image (Fig. 4, a-2, spots 1 and 2). The result that large big Ru^0 particles were observed from TEM image of Ru/SiO_2-r450 (Fig. 4, a-2) was coincided with the result of XRD characterization of the catalyst (Fig. 2, a-2). After Ru/SiO_2-c350 was employed in the hydrogenolysis of glycerol at 160 °C and 8.0 MPa H_2 for 8 h, it can be seen from the TEM image of spent Ru/SiO_2-c350 that fine Ru particles were spread on the surface of SiO_2, and the stick-shaped particles could not be observed on the spent catalyst (Fig. 4, a-3). EDX analysis (Fig. 4, a-3) showed higher intensities of Ru element in the dark regions (area 2 and area 3 in Fig. 4, a-3), while lower intensity of Ru element in the bright contrast region (area 1 in Fig. 4, a-3). Comparing the fine Ru^0 particles spread on spent Ru/SiO_2-c350 and the large Ru^0 particles on Ru/SiO_2-r450 from TEM images (Fig. 4, a-2 and a-3) and the XRD profiles (Fig. 2, a-2 and a-3), it is suggested that the aggregation of Ru^0 particles during the H_2 reduction was happened on Ru/SiO_2-r450.

In the case of $Ru–Re/SiO_2$-c350, a well spread and dispersed metal oxide particles (black area) could be seen from its TEM image (Fig. 4, b-1). Although the boundary of oxide metal particles was not clear, no stick particle or obvious aggregation can be observed. This indicates that the addition of Re component could promote the dispersion of RuO_2 on the surface of support SiO_2, which is consistent with the results of XRD (Fig. 2, a-1 and b-1). Both Ru and Re components were simultaneity co-existed on the surface of $Ru–Re/SiO_2$-c350 as proved by EDX analysis (Fig. 4, b-1).

On the other hand, after the pre-reduction of $Ru–Re/SiO_2$-c350, the sample of $Ru–Re/SiO_2$-r450 showed a certain extent aggregations of metal particles, and the distribution of particles on the surface of support SiO_2 was un-uniform (Fig. 4, b-2), although the dispersion of Ru species was promoted by the addition of Re component in comparison with the case of Ru/SiO_2-r450 (Fig. 4, a-2). When $Ru–Re/SiO_2$-c350 went through the reaction, it can be seen, from the TEM image of spent $Ru–Re/SiO_2$-c350 (Fig. 4, b-3), that the particles on the surface were fine and the aggregation of fine particles existed. In corresponding EDX analysis (Fig. 4, b-3) of spent $Ru–Re/SiO_2$-c350, the species of Ru and Re were detected in the analyzed regions of area 1 and 2 in Fig. 4, b-3.

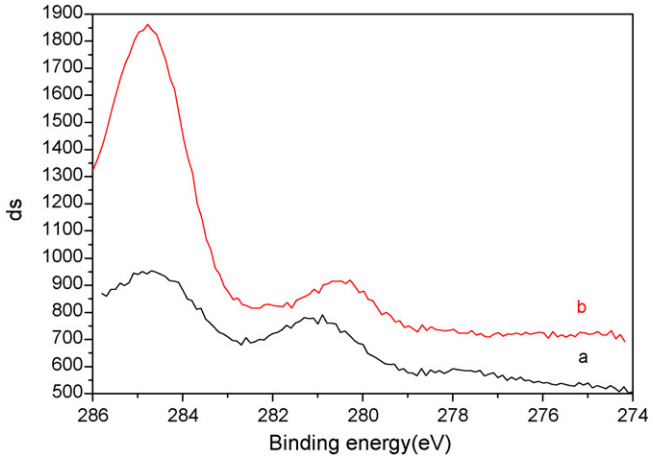

Fig. 5. XPS spectra of $Ru3d_{5/2}$ of (a) $Ru–Re/SiO_2$-c350, (b) spent $Ru–Re/SiO_2$-c350.

3.1.4. XPS characterization

In order to reveal the state of species Ru and Re in fresh and spent $Ru–Re/SiO_2$-c350, XPS measures was operated. As seen in the Fig. 5, Ru species in fresh $Ru–Re/SiO_2$-c350 showed the 281.0 eV binding energy (shorted as BE) of $Ru3d_{5/2}$. According to the reference book [30], the BE of $Ru3d_{5/2}$ of RuO_2 is in the range of 280.6–281.0 eV. This indicates that Ru species on fresh $Ru–Re/SiO_2$-c350 catalyst was in Ru^{4+} state. On the other hand, Ru species in the spent $Ru–Re/SiO_2$-c350 showed 280.4 eV BE, indicating that Ru species on spent $Ru–Re/SiO_2$-c350 was in Ru^0 metal state (the BE of $Ru3d_{5/2}$ of Ru^0 is in the range of 279.9–280.2 eV [30]). The change of the state of Ru species from RuO_2 in fresh $Ru–Re/SiO_2$-c350 to Ru^0 in spent $Ru–Re/SiO_2$-c350 coincided with the result of XRD (Fig. 2, b-1 and b-3).

The BE of $Re4f_{7/2}$ of Re species in the fresh $Ru–Re/SiO_2$-c350 was 45.3 eV (Fig. 6a). From the reference book, the BE of $Re4f_{7/2}$ of ReO_3 is in the range of 46.6–47.0 eV and the BE of $Re4f_{7/2}$ of ReO_2 is in the range of 43.4–43.9 eV [30]. Making allowance for the error caused by fitting process, Re species in fresh $Ru–Re/SiO_2$-c350 should be in oxide state, mostly in ReO_3 state. The difference in the BE of $Re4f_{7/2}$ of ReO_3 between fresh $Ru–Re/SiO_2$-c350 and reference data might be due to the interaction of Ru and Re species on the surface of $Ru–Re/SiO_2$-c350. On the other hand, the BE of $Re4f_{7/2}$ of Re species in spent $Ru–Re/SiO_2$-c350 was 45.9 and 40.9 eV and the area ratio of two peaks was 33.3/23.8, which was calculated from the fitting curves. The BE of $Re4f_{7/2}$ of Re^0 is in the range of 40.3–40.9 eV [30].

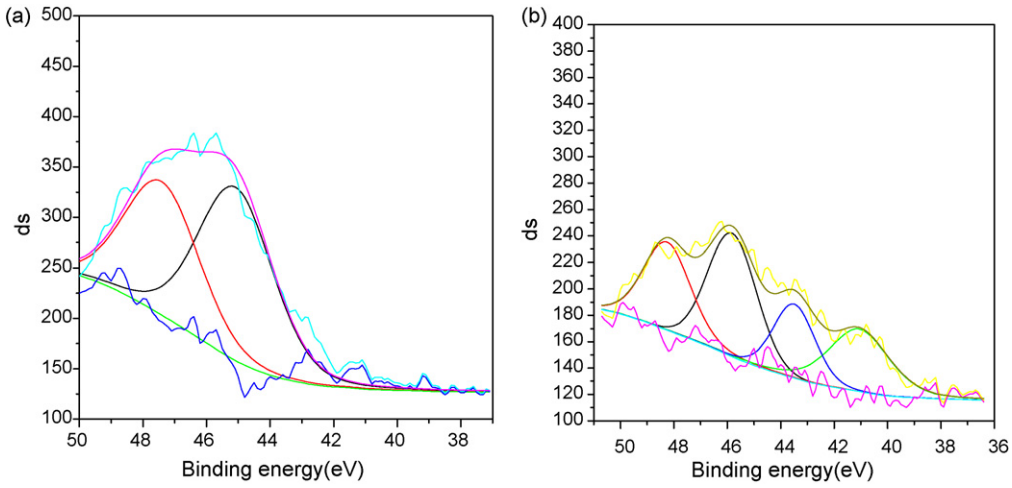

Fig. 6. XPS spectra of $Re4f_{7/2}$ observed and calculated by curve fitting of (a) $Ru–Re/SiO_2$-c350, (b) spent $Ru–Re/SiO_2$-c350.

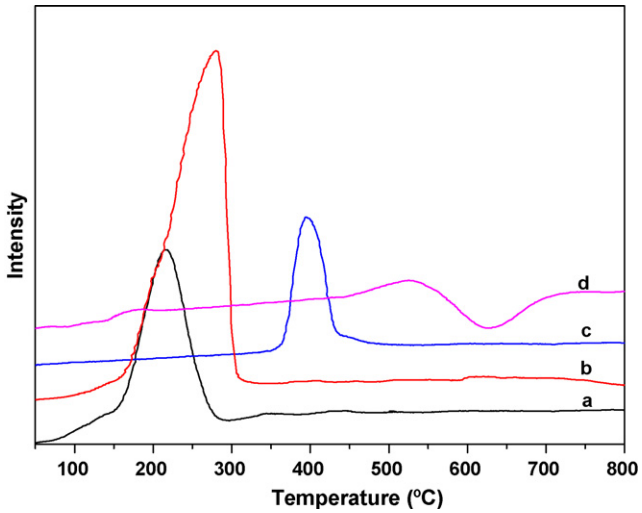

Fig. 7. TPR profiles of (a) Ru/SiO_2-c350, (b) Ru–Re/SiO_2-c350, and (c) Re/SiO_2-c350, and (d) spent Ru-Re/SiO_2-c350 (after reaction). (Data of (a), (b) and (c) are from reference [24]).

This implies that small part of ReO_3 in fresh Ru–Re/SiO_2-c350 was reduced into Re^0 after undergoing the hydrogenolysis of glycerol, while most of Re species was still in ReO_3 state.

3.1.5. Catalyst reducibility and dispersion

The reduction behaviors of Ru/SiO_2-c350, Re/SiO_2-c350, Ru–Re/SiO_2-c350 and spent Ru-Re/SiO_2-c350, as well as the interaction of Ru and Re on Ru–Re/SiO_2-c350 were investigated with H_2-TPR, and the results are shown in Fig. 7. The H_2-TPR profile of Ru/SiO_2-c350 showed one reduction peak at 215 °C (Fig. 7a), which was assigned to the reduction of Ru species from RuO_2 to Ru^0 [26]. Re/SiO_2-c350 also showed only one reduction peak at 396 °C, which was attributed to the reduction of rhenium oxide [31,32]. On the other hand, in the H_2-TPR profile of Ru–Re/SiO_2-c350, one strong and broad peak was appeared, in which the reduction temperature (279 °C) was lower than that (396 °C) in Re/SiO_2 H_2-TPR and higher than that (215 °C) in Ru/SiO_2 H_2-TPR. These results suggest that the interaction between Ru and Re on the surface of Ru–Re/SiO_2-c350 occurred, and the reduction behavior of bimetallic Ru–Re/SiO_2-c350 was different from corresponding monometallic Ru/SiO_2-c350 and Re/SiO_2-c350. The quantities of H_2 consumption per gram catalyst were calculated and the results showed that the H_2 consumption of Ru/SiO_2, Re/SiO_2 and Ru–Re/SiO_2 catalysts are 0.435, 0.349 and 0.814 mmol/g, respectively. On the other hand, the TPR profile of spent Ru-Re/SiO_2-c350 (Fig. 7d) showed a gradual reduction behavior starting from 100 °C, and a reduction peak centered at about 525 °C was observed in the TPR profile of spent Ru-Re/SiO_2-c350. This result indicates that Re component might be in oxidative state in the spent Ru-Re/SiO_2-c350 after the reaction, and some interaction between Re component and support happened during the reaction.

The dispersion of Ru metal on support SiO_2 was measured by CO chemisorption, and CO uptake (the molar ratio of CO/Ru) on Ru/SiO_2-c350 or Ru–Re/SiO_2-c350 catalysts during CO pulse chemisorption is shown in Table 2. The molar ratio of CO/Ru over Ru/SiO_2-c350 was low (CO/Ru = 0.046), indicating the dispersion of Ru on SiO_2 was not well (Table 2, No. 1). This is coincident with the characterized results from XRD, TPR and TEM. As mentioned above, the XRD pattern of Ru/SiO_2-c350 showed sharp diffraction peaks (Fig. 2, a-1), and the H_2-TPR profile of Ru/SiO_2-c350 revealed one intensive reduction peak (RuO_2 to Ru^0), indicating the existence of crystallized RuO_2 on the surface of SiO_2. When Ru and Re components were simultaneously supported on SiO_2, the CO/Ru uptake over Ru–Re/SiO_2-c350 increased remarkably (Table 2, No. 2), suggesting that Ru–Re particles were relatively well dispersed on the surface of SiO_2. The CO chemisorption on Re/SiO_2-c350 was also performed to estimate the contribution of Re component during the CO chemisorption on Ru–Re/SiO_2-c350. The result showed that the CO uptake on Re/SiO_2-c350 was very low (Table 2, No. 5) after that the sample was pretreated in H_2 at 400 °C. When Ru–Re/SiO_2-c350 was pretreated in H_2 at lower temperature 300 or 200 °C before CO chemisorption, the CO uptake increased (Table 2, Nos. 3 and 4). These results imply that the dispersion of Ru metal on Ru–Re/SiO_2-c350 was related with the pre-reduction temperatures of the sample, and higher reduction temperatures might cause the aggregation of Ru metal on the catalyst surface.

Table 2
Total CO uptake on Ru/support and Ru–Re/support in CO pulse chemisorptions.

No.	Catalyst	CO/Ru molar ratio (Ru dispersion)
1	Ru/SiO_2-c350[a]	0.046
2	Ru–Re/SiO_2-c350[a]	0.23
3	Ru–Re/SiO_2-c350[b]	0.34
4	Ru–Re/SiO_2-c350[c]	0.39
5	Re/SiO_2-c350[a]	0.005

[a] Treated in a flow of pure H_2 at 400 °C before CO pulse chemisorption.
[b] Treated in a flow of pure H_2 at 300 °C before CO pulse chemisorption.
[c] Treated in a flow of pure H_2 at 200 °C before CO pulse chemisorption (Data of No. 1 and 2 are from reference [24]).

3.2. Hydrogenolysis of glycerol

The prepared Ru–Re/SiO_2 and Ru/SiO_2 catalysts were tested for their catalytic performances in the hydrogenolysis of glycerol, and the reaction products were 1,3-propanediol (1,3-PDO), 1,2-propanediol (1,2-PDO), 1-propanol (1-PO), 2-propanol (2-PO), ethyl glycol (EG), ethanol and methanol (Table 3). In our previous research, we found a prominent promoting effect of $Re_2(CO)_{10}$ on the activity of Ru monometallic catalysts in glycerol hydrogenolysis to propanediols, and the influence of reaction conditions (reaction temperature, hydrogen pressure and reaction time, etc.) on catalytic performance has also been examined [23]. Therefore, 160 °C, 8.0 MPa and 8 h were chosen as the standard reaction conditions in present study.

In present study, the promoting effect of $Re_2(CO)_{10}$ on Ru/SiO_2-c350 and Ru/SiO_2-r450 were investigated firstly. Although the calcined catalyst Ru/SiO_2-c350 showed higher activity in glycerol hydrogenolysis than the pre-reduced catalyst Ru/SiO_2-r450 (Table 3, Nos. 1 and 3), the promoting effect of $Re_2(CO)_{10}$ was obvious on both of them (Table 3, Nos. 1, 2 and 3, 4). The conversion of glycerol increased 2.2 and 4.0 times, respectively. Moreover the selectivity of propanediols increased and the selectivity of degradation product, ethylene glycol, decreased obviously. These results are coincident with the regularity of the promoting effect of $Re_2(CO)_{10}$ in our previous study [23].

The bimetallic Ru–Re/SiO_2 catalysts, which were pretreated under different conditions, were employed in glycerol hydrogenolysis, and their activities were compared with Ru/SiO_2 catalyst. As expected, Ru–Re/SiO_2-c350 showed much higher activity and less selectivity to degradation product (ethylene glycol) than Ru/SiO_2-c350 (Table 3, Nos. 1 and 6). As shown in Table 3 (No. 5), Re/SiO_2 showed very low catalytic activity (the conversion of glycerol was merely 1.7%). This result confirmed that Re species alone did not possess the catalytic activity for glycerol hydrogenolysis and further testified that there existed a synergistic effect between species Ru and Re in the case of Ru–Re/SiO_2 catalyst or Ru/SiO_2 + $Re_2(CO)_{10}$ system.

Table 3
Effect of pretreatment of catalysts on the catalytic performance of Ru–Re/SiO_2 catalysts in glycerol hydrogenolysis[a].

No.	Catalyst	Conversion (%)	Selectivity (%)						
			MeOH	EtOH	EG	1-PO	2-PO	1,2-PDO	1,3-PDO
1	Ru/SiO_2-c350	16.8	0.8	6.3	18.2	27.2	2.1	39.0	6.4
2	Ru/SiO_2-c350 + $Re_2(CO)_{10}$	37.0	0.2	3.4	5.4	24.2	4.4	51.7	10.7
3	Ru/SiO_2-r450	3.8	0.9	3.7	19.5	1.9	25.3	40.5	8.1
4	Ru/SiO_2-r450 + $Re_2(CO)_{10}$	15.3	0.3	3.2	6.1	3.9	23.1	44.4	11.0
5	Ru–Re/SiO_2-c350	51.7	0.4	8.4	6.4	29.1	6.7	44.8	4.2
6	Ru–Re/SiO_2-r200	51.0	0.2	5.8	4.8	26.1	5.6	49.1	8.3
7	Ru–Re/SiO_2-r300	47.5	0.2	4.6	4.9	26.2	5.2	49.5	9.4
8	Ru–Re/SiO_2-r450	23.8	0.2	2.5	6.1	23.0	3.5	51.1	13.6
9	Re/SiO_2-c350	1.7	2.1	6.2	11.4	20.9	6.8	44.4	8.1
10	$Re_2(CO)_{10}$[b]	1.2	2.4	4.5	12.5	14.9	15.1	38.8	11.7

[a] Reaction conditions: 160 °C, 8 MPa H_2, 8 h, 10 ml 40 wt% glycerol aqueous solution, 150 mg Ru/support catalyst, molar ratio of Ru/Re = 1.
[b] $Re_2(CO)_{10}$ = 0.0242 g (Data of No. 1, 2, 5 and 9 are from reference [24]).

As mentioned above, the pretreatment of catalyst precursors could change the physicochemical properties of the catalysts, which could in turn influence the catalytic performance of the catalysts in the reaction. The effects of calcinations and pre-reduction temperatures on the activity of bimetallic Ru–Re/SiO_2 catalysts were compared. No matter for Ru/SiO_2 monometallic or Ru–Re/SiO_2 bimetallic catalyst, reduction at high temperatures showed inhibition effect on the activity of the catalysts. For instance, the glycerol conversion was 16.8% over Ru/SiO_2-c350, while it decreased to 3.8% over Ru/SiO_2-r450 (Table 3, Nos. 1 and 3), which was obtained by pre-reducing in H_2 flow at 450 °C. The same tendency happened to Ru–Re/SiO_2 bimetallic catalyst, and glycerol conversion was 51.7% over Ru–Re/SiO_2-c350 whereas 23.8% over Ru–Re/SiO_2-r450.

Considering the adverse effect of high reducing temperature on the dispersion of active metal, it is desired to pre-reduce the catalysts at lower temperature. From the results of XRD, RuO_2 species in Ru/SiO_2-c350 and Ru–Re/SiO_2-c350 catalysts (Fig. 2, a-1 and b-1) were testified to be in-situ reduced to Ru^0 (Fig. 2, a-3 and b-3) during glycerol hydrogenolysis under the reaction condition of 160 °C, 8MPa H_2 and 8 h. TPR results also showed that RuO_2 in Ru/SiO_2 could be reduced at the temperatures between 200 and 300 °C. Therefore, the temperatures of 200 and 300 °C were selected for the pre-reduction of Ru–Re/SiO_2 in H_2 flow.

As it can be seen from the results in Table 3, Nos. 6–8, the conversion of glycerol increased with the decrease of pre-reduction temperature of Ru–Re/SiO_2-c350 catalyst. Especially when the pre-reduction temperature decreased from 450 to 300 °C, glycerol conversion increased from 23.8% to 47.5%. When the pre-reduction temperature decreased from 300 to 200 °C, glycerol conversion increased from 47.5% to 51.0%, although it was not obvious. These results imply that, if pre-reduction temperatures were below 400 °C, the synergic effect between species Ru and Re would become more efficient, even though not as efficient as the case of in-situ reduction of the calcined sample Ru–Re/SiO_2-c350. And result of CO chemisorption testified the similar conclusion that decreasing the pre-reduction temperature from 400 to 300 °C would evidently increase the dispersion of Ru/CO (Table 2, Nos. 3 and 4). Related with the result of TPR that the reducing temperature of rhenium oxide on Re/SiO_2-c350 was 396 °C, rhenium oxide in Re/SiO_2-c350 was not easy to be reduced to Re^0 state during the reaction. From the result of XPS, most of rhenium oxide in spent Ru–Re/SiO_2-c350 still remained oxide state after the reaction. Therefore, it is suggested that Re component was probably in rhenium oxide state rather than Re^0 metal state to take part in the reaction via interaction with Ru^0 metal. Low temperature reduction or in-situ reduction could prevent the over-reduction of Re species and the growth of Ru^0 particles, and also be favor the interaction of rhenium oxide and ruthenium metal.

In glycerol hydrogenolysis to propanediols, the key pathways may involve glycerol dehydration on acid sites to acetol or 3-hydroxypropionaldehyde and the hydrogenation of the intermediate on metal sites to 1,2-propanediol or 1,3-propanediol [4]. It is suggested that the synergistic effect between hydrogenation sites and acid sites on the surface of the catalysts might be a possible promoting mechanism for Ru–Re/SiO_2 catalysts. It has been reported that rhenium oxide showed surface acidity, and this has been proved by the characterization of IR spectra of pyridine adsorption and NH_3-TPD [33,34]. Therefore, for Ru–Re catalysts, rhenium oxide species would act as a solid acid and it could promote the glycerol dehydration step, and subsequently increase the activity of Ru–Re catalysts and the selectivity of PDO. ReOx with acid sites synergized with Ru^0 hydrogenation sites on the surface of Ru–Re catalyst, and this synergistic effect promoted the activity of the catalysts.

4. Conclusion

Bimetallic Ru–Re/SiO_2 showed higher activity (51.7% conversion) than monometallic Ru/SiO_2 catalyst (16.8% conversion) in the hydrogenolysis of glycerol under the reaction conditions of 160 °C, 8.0 MPa and 8 h. Re/SiO_2 alone had almost no activity (1.7% conversion), but adding Re component into Ru/SiO_2 could obviously promote the activity of the catalysts. The different pretreatment of the catalyst precursors had great influence on the catalytic performance of both Ru–Re/SiO_2 and Ru/SiO_2 catalysts. High pre-reduction temperature (450 °C) in H_2 flow accelerated the aggregation of particles and decreased the dispersion of metal components on SiO_2, which in turn decreased the catalytic performance of Ru–Re/SiO_2 and Ru/SiO_2. It is suggested that Ru species might be in Ru^0 metal state, while Re species might mostly be in rhenium oxide state during the hydrogenolysis of glycerol. Low temperature reduction (<300 °C) or in-situ reduction could prevent the over-reduction of Ru species and the growth of Ru^0 particles, and would be favor the interaction of rhenium oxide and ruthenium metal.

Acknowledgment

This work is supported by the Analytical Foundation of Tsinghua University, China. Authors are grateful of Mr. Zhanping Li for his discussion and advice on XPS measurements.

References

[1] A. Behr, J. Eilting, K. Irawadi, J. Leschinski, F. Lindner, Green Chem. 10 (2008) 13.
[2] J.N. Chheda, G.W. Huber, J.A. Dumesic, Angew. Chem. Int. Ed. 46 (2007) 7164.
[3] J. Chaminand, L. Djakovitch, P. Gallezot, P. Marion, C. Pinel, C. Rosier, Green Chem. 6 (2004) 359.
[4] T. Miyazawa, Y. Kusunoki, K. Kunimori, K. Tomishige, J. Catal. 240 (2006) 213.
[5] S. Demirel-Gulen, M. Lucas, P. Claus, Catal. Today 102–103 (2005) 166.

[6] S.H. Chai, H.P. Wang, Y. Liang, B.Q. Xu, Green Chem. 9 (2007) 1130.
[7] J. van Haveren, E.L. Scott, J. Sanders, Biofuels Bioprod. Biorefin. 2 (2008) 41.
[8] M. Dasaria, P. Kiatsimkula, R. Sutterlinb, G. Suppesa, Appl. Catal. A 281 (2005) 225.
[9] P. Alvise, T. Pietro, Ind. Eng. Chem. Res. 44 (2005) 8535.
[10] T. Miyazawa, S. Koso, K. Kunimori, K. Tomishige, Appl. Catal. A 318 (2007) 244.
[11] T. Kurosaka, H. Maruyama, I. Naribayashi, Y. Sasaki, Catal. Commun. 9 (2008) 1360.
[12] E.P. Maris, W.C. Ketchie, M. Murayama, R.J. Davis, J. Catal. 251 (2007) 281.
[13] E.P. Maris, R.J. Davis, J. Catal. 249 (2007) 32.
[14] V.D. Stytsenko, Appl. Catal. A 126 (1995) 1.
[15] M. Ronning, T. Gjervan, R. Prestvik, D.G. Nicholson, A. Holmen, J. Catal. 204 (2001) 292.
[16] Yu.V. Guryev, I.I. Ivanova, V.V. Lunin, W. Grunert, M.W.E. van den Berg, Appl. Catal. A 329 (2007) 16.
[17] F. Epron, F. Gauthard, J. Barbier, Appl. Catal. A 237 (2002) 253.
[18] H. Zhang, G.P. Cao, Z.Y. Wang, Y.S. Yang, Z.J. Shi, Z.N. Gu, J. Phys. Chem. C 112 (12) (2008) 4524.
[19] Z.Q. Zhu, Z.H. Lu, B. Li, S.Z. Guo, Appl. Catal. A 302 (2006) 208.
[20] J.N. Coupe, E. Jordao, M.A. Fraga, M.J. Mendes, Appl. Catal. A 199 (2000) 45.
[21] Z. Paal, N. Gyorffy, A. Wootsch, L. Toth, I. Bakos, S. Szabo, U. Wild, R. Schlogl, J. Catal. 250 (2007) 254.
[22] J.M. Rynkowski, T. Paryjczak, M. Lenik, Appl. Catal. A 126 (1995) 257.
[23] L. Ma, D.H. He, Z.P. Li, Catal. Commun. 9 (2008) 2489.
[24] L. Ma, D.H. He, Top. Catal., doi:10.1007/s11244-009-9231-3.
[25] W.F. Han, H.Z. Liu, H. Zhu, Catal. Commun. 8 (2007) 351.
[26] R. Lanza, S.G. Jaras, P. Canu, Appl. Catal. A 325 (2007) 57.
[27] I.E. Wachs, Catal. Today 27 (1996) 437.
[28] Y.M. Chen, A. Korotcov, H.P. Hsu, Y.S. Huang, D.S. Tsai, New J. Phys. 9 (2007) 130.
[29] Y. Liu, F.Y. Huang, J.M. Li, W.Z. Weng, C.R. Luo, M.L. Wang, W.S. Xia, C.J. Huang, H.L. Wan, J. Catal. 256 (2008) 192.
[30] F.M. John, F.S. William, E.S. Peter, D.B. Kenneth, Handbook of X-ray Photoelectron Spectroscopy, Physical Electronics, Inc., Minnesota, USA, 1995.
[31] G. Jacobs, J.A. Chaney, P.M. Patterson, T.K. Das, B.H. Davis, Appl. Catal. A 264 (2004) 203.
[32] J.P. Breen, R. Burch, K. Griffin, C. Hardacre, M. Hayes, X. Huang, S.D. O'Brien, J. Catal. 236 (2005) 270.
[33] T. Kawai, K.M. Jiang, T. Ishikawa, J. Catal. 159 (1996) 288.
[34] F.S. Nahama, O. Clause, D. Commereuc, J. Saussey, Appl. Catal. A 167 (1998) 237.